Journal of the Australian Ceramic Society
https://doi.org/10.1007/s41779-025-01176-1

RESEARCH

Characterization and crystallization mechanism of SiO_2-Al_2O_3-Li_2O glass–ceramic using non-isothermal models

Abdelheq Layachi[1,2] · Soufyane Satha[3] · Maurice François Gonon[4] · Hamid Satha[1]

Received: 28 May 2024 / Revised: 18 February 2025 / Accepted: 26 February 2025

Abstract
In this paper we investigate the impact of ZrO_2 and TiO_2 as nucleating agents on the crystallization behavior of a lithium aluminosilicate (LAS) glass–ceramic (G-C). The crystallization mechanism is explored at first through X-ray diffraction analyses next to various heat treatments. Differential scanning calorimetry (DSC) analyses conducted under non-isothermal conditions at different heating rates reveal well-defined exothermic peaks. The activation energy (*Ea*), the key parameter in understanding thermal kinetics, is determined through model-free methods, specifically Flynn Wall Ozawa (FWO) and Kissinger Akahira Sunose (KAS), as well as the model-fitting approach (Coats-Redfern, C–R method). Additionally, the crystallization mechanism of the studied LAS glass ceramic is discussed utilizing the C–R method and Criado's methods. By employing these techniques, a comprehensive analysis of the LAS glass–ceramic system is provided, contributing to the fundamental understanding of its crystallization processes, and laying the groundwork for further advancements in G–C materials.

Keywords Glass–ceramic (G-C) · LAS · Crystallization · Non-isothermal · DSC · Activation energy (Ea)

Introduction

Glass–ceramic materials are a type of advanced materials that is prepared through the controlled crystallization of glasses. This process involves subjecting a glass composition to controlled heat treatment, leading to the development of crystalline phases within the amorphous glass matrix. Glass–ceramics exhibit a combination of properties that makes these materials well suited for applications where both dimensional stability and resistance to thermal shock are essential [1]. The Li_2O–Al_2O_3–SiO_2, known as lithium aluminosilicate (LAS), system, stands out as the most commercially successful among various glass–ceramic systems. These materials are commonly employed as substrates for microelectronic packaging and microwave dielectrics [2–6], and primarily attributed to their remarkable thermal properties, characterized by a low thermal expansion coefficient and a high upper operating temperature [7, 8].

Nucleation agents, such as ZrO_2 and TiO_2, are employed for inducing controlled bulk crystallization in the parent glass [9–11]. In commercial LAS glass–ceramics, supplementary components are typically incorporated to decrease glass melting temperatures, cut down on batch costs, and expand the working range [9, 10]. These two oxides can incorporate into the β-spodumene crystals through partial solid solution, effectively minimizing thermal expansion, acting as a glass flux, and reducing batch material costs [9, 12–15]. The most commonly used nucleating agents are ZrO_2, TiO_2 oxides, and their mixtures, which demonstrate enhanced performance in grain refinement due to the formation of $ZrTiO_4$ [16–18]. For instance, Höche T et al. [19] investigated the effect of ZrO_2 and TiO_2 on the nucleation mechanism in lithium aluminosilicate glass. Furthermore, the influence of P_2O_5 oxides has been specifically studied in LAS glass–ceramics. A. de Pablos-Martín et al. [20] and Xingzhong Guo et al. [21] examined

✉ Abdelheq Layachi
layachi.abdelheq@umc.edu.dz

✉ Hamid Satha
satha.hamid@univ-guelma.dz

1 Laboratoire LSPN, Universitédu 8 Mai 1945 Guelma, BP 401, Guelma, Algérie

2 Université Mentouri Constantine: Universite Constantine 1, ISTA, Constantine 25000, Algérie

3 Université Polytechnique Hauts-de-France, CERAMATHS, 59313 Valenciennes, France

4 Materials Institute, University of Mons, Rue de L'Epargne 56, 7000 Mons, Belgium

Published online: 20 March 2025

the crystallization mechanism using the calculated Avrami exponent according to DSC curves at various heating rates. Additionally, the inclusion of MgO plays a role in lowering the crystallization temperature and aiding the phase transformation from β-quartz to β-spodumene in the LAS glass–ceramics system [22]. It is well-established that heat-treatment time and temperature play crucial roles in determining the final structure and properties of glass–ceramics. Thermal analysis, a quick and convenient method, proves useful in examining the kinetics of chemical reactions and the crystallization processes in glass [23]. This technique has been applied to investigate the crystallization kinetics in diverse glass systems, including LAS [24–30].

This study aims to investigate how the addition of TiO_2 and ZrO_2 affects the thermal behavior, kinetics, and mechanism of crystallization in a lithium-aluminosilicate (LAS) glass–ceramic. The investigation employs a non-isothermal method using DSC. Additionally, the objective is to determine if the activation energy (Ea) correlates consistently with the degree of conversion and the appropriateness of the proposed methods.

Utilizing model-free techniques like FWO and KAS, as well as model-fitting methods such as C-R, the E_a of LAS G-C was assessed. Additionally, Master plot methods, including C-R and Criado's methods, were applied to identify potential reaction models for LAS G-C. This approach contributes to a deeper understanding of the thermal crystallization mechanism linked to LAS G-C.

Experimental procedure

The glass, with a nominal composition of SiO_2-Al_2O_3-Li_2O-TiO_2-ZrO_2-MgO-ZnO, was prepared by the Centre de Recherche Corning Europe using the conventional melt quenching method. This material was provided to us as a disk with a diameter of 20 cm and a thickness of 5 mm. The glass was annealed for 1h at 600 °C to relax internal stresses [31]. The oxide weight fractions of the glass are provided in Table 1.

Analytical methods

The glass–ceramic was pulverized by agate ball milling (Ball mill PM100, from Germany), resulting glass–ceramic powder for use in thermal analysis. The glass transition temperature (T_g) and crystallization temperature (T_c) were determined using a DSC (Netzsch STA449C model, from Germany) using samples of mass in the range 30–40 mg. The sample was placed in platinum pans within the sample oven, whereas an empty pan was set in the reference oven. The thermal cycle consisted in heating the sample at different rates ($\beta = 5$, 10, 15, 20, 25, 30, 35 and 40 °C/min) from room temperature to 1200 °C with a temperature error of ± 5 °C.

Confirmation of the amorphous nature of the glass and the crystal phases present in the corresponding G-Cs was achieved through X-ray diffraction, using a D8 ADVANCE ECO Bruker model from Germany. Under operating conditions (40kV, 20 mA and Copper anticathode Wavelength (Kα1) = 0.154 nm). The scanning conditions include a step size of 0.02° at a rate of 2°/min, covering an angle range of 2θ from 10° to 80°.

The method introduced by Krimm et al., [32], was employed to estimate the crystallinity index. This method calculates crystallinity as the ratio of the diffracted crystalline area (Ac) to the total diffracted area (AT = crystalline area + amorphous area), as defined by Eq. 1.

$$CrI\% = \left(\frac{A_c}{A_c + A_a}\right) \times 100 \tag{1}$$

where CrI = crystallinity index (%); Ac = diffracted crystalline area; Aa = diffracted amorphous area.

The Vickers hardness was assessed utilizing a micro hardness tester (DHV-1000, China). A minimum of four points were measured per sample to calculate the average hardness, with an error margin of ± 0.2 GPa.

The H_v hardness is assessed through the ratio of applied load (P) divided to surface area (A). Where, P, d and A represents, respectively, the load applied to the material's surface, mean diagonal and the surface area measured in square micrometers [33–36]. The determination of A involves the application of the following formula:

$$A = \frac{d^2}{2sin\left(\frac{136°}{2}\right)} \tag{2}$$

$$A \approx \frac{d^2}{1.8544} \tag{3}$$

In this study, the Vickers microhardness test method to measure hardness. The measurements utilized a pyramid-shaped indentation tip with an apex angle (α) of 136°. Vickers microhardness values (Hv) were calculated under a load of 100 g for a peak-load time of 10 s, using Eq. 4.

Table 1 Composition of the glass samples (wt.%)

SiO_2	Al_2O_3	Li_2O	TiO_2	ZrO_2	MgO	ZnO
69%	20%	3	2,5	2,5	2	1

$$Hv = 1.8544\frac{P}{d^2} \tag{4}$$

$$E = 81.9635H_v \tag{5}$$

The constant 81.9635 in Eq. 5 is employed for the calculation of elastic modulus in ceramic materials, as specified in [33, 34].

The yield strength (Y) represents the maximum stress a material can endure without undergoing plastic deformation, and it can be determined using Eq. (6) [35, 36].

$$Y \approx \frac{H_v}{3} \tag{6}$$

Yield strength holds significant importance in the structural design of engineering applications. When designing a device, it becomes imperative to ensure that the material chosen possesses ample yield strength to support the applied load without undergoing plastic deformation.

Results and discussion

DSC and thermal data

Figure 1 illustrates the DSC curves of glass subjected to varying heating rates. A wide endothermic stage, associated to the glass transition, is observed within the temperature range of 730 °C to 750 °C. The T_g for each heating rate was determined during this stage. Notably, all curves displayed a distinct exothermic peak, suggesting that a suitable heat treatment would induce the precipitation of micro-crystals from the parent glass.

The glass's formability was evaluated by analyzing the thermal parameters ΔT and S, as specified by Dietzel and Saad Paulin [37, 38].

$$\text{Dietzel}: \ \Delta T = Tc - Tg \tag{7}$$

$$\text{Saad} - \text{Paulinl}: \ S = (Tc - To)(To - Tg)/Tg \tag{8}$$

where T_g, T_c, and T_o represent the glass transition temperature, crystallization peak temperature, and crystallization onset temperature, respectively—all obtained from the DSC curves—the glass stability is assessed based on the values of ΔT and S. The higher values of ΔT and S indicate greater resistance to crystallization during heating, reflecting enhanced thermal stability. This means the glass can maintain its amorphous state over a wider temperature range before crystallization begins. These parameters provide insights into the thermal behavior of the glass and its resistance to crystallization, making them useful indicators in assessing the overall stability of the material. For a more convenient comparison, the characteristic temperatures of the glass are compiled in Table 2.

X-ray analysis (XRD)

When the glass is subjected to heat treatment at 800°C for various dwell times, the X-ray diffraction analyses, reveal that no diffraction peaks are observed until the sample undergoes a 2-h treatment (Fig. 2). This absence of diffraction peaks suggests that the glass is in an amorphous state

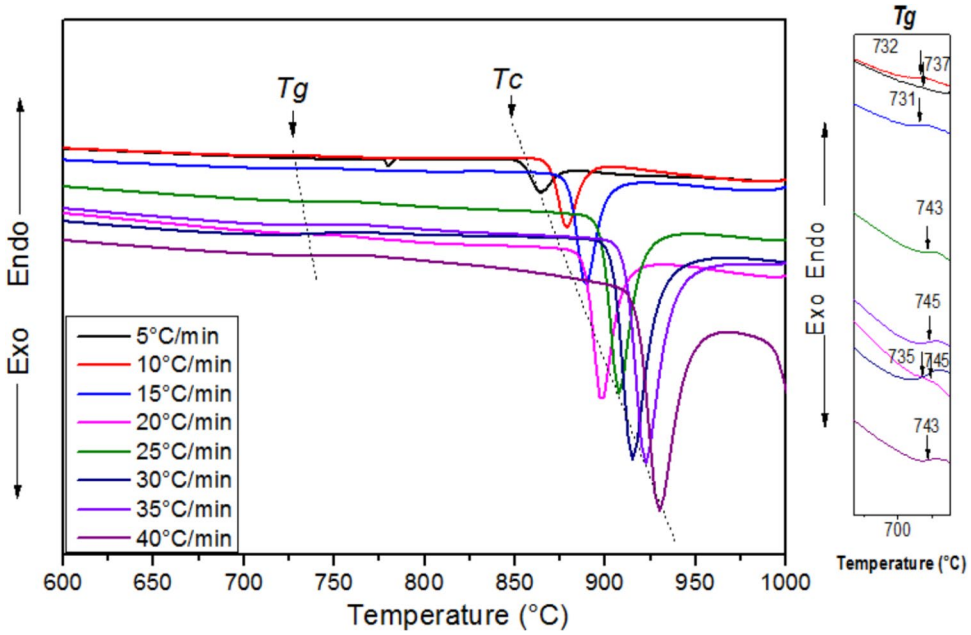

Fig. 1 (DSC) curves for different heating rates

Table 2 *Tg*, *Tc*, and *To* temperatures, as well as parameters (ΔT and *S*)

β (°C /min)	*Tg (°C)*	*To(°C)*	*Tc (°C)*	*ΔT(°C)*	*S*
5	737	850	864	127	2,15
10	732	863	879	147	2,86
15	731	873	889	158	3,11
20	735	880	898	163	3,55
25	743	889	907	164	3,54
30	745	895	915	170	4,03
35	745	903	923	178	4,24
40	743	908	928	185	4,44
Error	±3	±3	±3	±3	±0,01

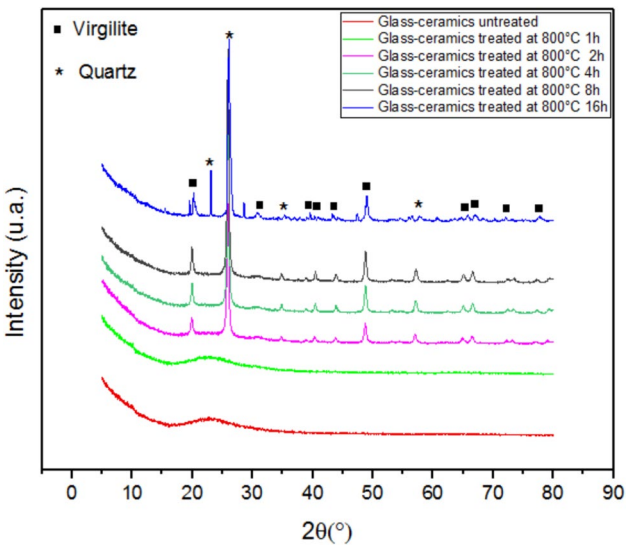

Fig. 2 XRD of sample various heat-treatment time and temperatures

initially. However, after the 2-h mark, diffraction peaks become evident, indicating the initiation of crystallization.

The initiation of crystallization at approximately 800°C, consistent with the first crystallization peak observed in the DSC results, implies that the heat treatment induces a transformation from an amorphous to a crystalline state. The DSC results provide additional insight into the thermal behavior of the glass, corroborating the X-ray diffraction findings and enhancing our understanding of the phase changes occurring during the heat treatment process [39, 40].

At 800°C for 2 h, an additional broad peak becomes apparent, identified as stemming from the presence of a $ZrTiO_4$ crystalline phase. If the time of heat treatment is greater than two hours, several new and sharp peaks appear. These fresh peaks were recognized as closely associated with the virgilite crystalline phase ($Li_x\ Al_x\ Si_{3-x}\ O_6$), and some quartz were observed. This observation aligns with the characterization of crystalline phases in silicoaluminate glasses, as described in prior work [29, 31].

The crystallization process can be summarized in four key stages, according to heat treatment applied to the glass–ceramic (Fig. 3):

The first stage corresponds to precipitation with formation tiny germs, or nuclei, form within the glass matrix, primarily composed of $ZrTiO_4$. This stage is facilitated by the presence of TiO_2 and ZrO_2, which are well-known nucleating agents that lower the energy barrier for nucleation. The nucleation of these crystallites is reported to be quite easy, leading to a significant number of initial germs.

The second stage correspond to coalescence of crystals: the initial crystals undergo coalescence, where they begin to merge. During this stage, the number of crystals decreases as they coalesce, and the average size of the crystals increases, reaching a diameter of approximately 55 Å [31]. This increase in crystal size marks a shift towards a more stable structure, essential for subsequent growth and transformation stages.

Next, crystalline phase forms around the coalesced crystals. According to ASTM data, this phase is identified as virgilite ($LiAlSiO_4$, a lithium aluminosilicate). The appearance of virgilite indicates a transformation in the

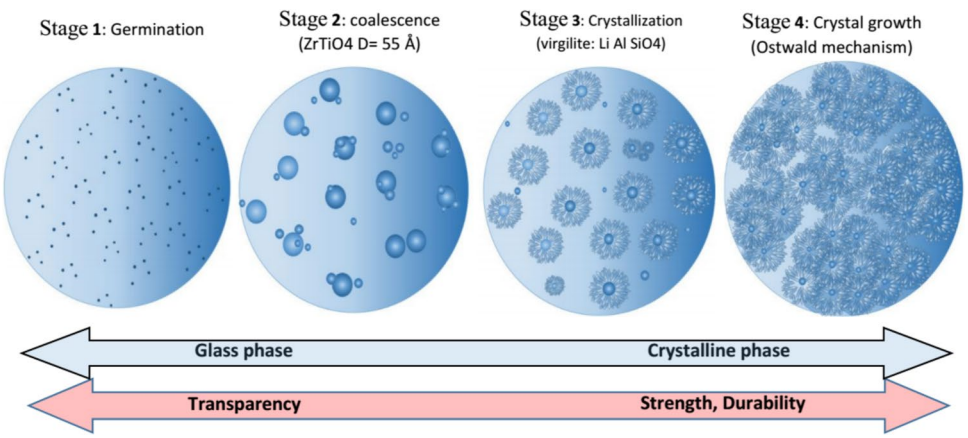

Fig. 3 The stages of crystallization of glass ceramics

microstructure, with the development of distinct crystalline regions surrounding the initial $ZrTiO_4$-based germs.

Finally, Crystal growth continues as a function of the heat treatment time. Following the Ostwald ripening mechanism, smaller crystals dissolve, and larger crystals grow, leading to an increase in the size of crystallized domains. As a growth progresses, the crystalline regions become large enough to interpenetrate.

According to the results obtained from TiO_2-containing glasses, it is quite evident that TiO_2 is greatly effective in the nucleation and crystallization processes. Several investigators [41, 42] have demonstrated that in glasses with substantial TiO_2 content, the effective nuclei and small titanium crystallites are composed of compounds such as TiO_2 itself or titanates.

TiO_2 preferentially promoted the nucleation of the keatite structure, facilitating the transformation of β-quartz ss into keatite ss, while ZrO_2 primarily nucleated or stabilized the high-quartz structure in Li_2O–MgO–Al_2O_3–SiO_2 glasses nucleated with TiO_2, ZrO_2, or both [41].

Fernandes, H. R. et al. [42], provided important insights into the crystallization mechanism the contribution of (TiO_2 and ZrO_2) on the crystallization behavior and the properties of glasses. Moreover, the occurrence of liquid–liquid phase separation was observed in all experimental compositions with some specific and delicate differences, which exert a strong influence in the phase composition and microstructure of G–C.

Mechanical properties

Table 3 illustrates the impact of heat-treatment time and temperature on the crystallinity index and mechanical properties (*Hv*, *E*, and *Y*) of the G–C. As depicted in Fig. 2, with the rise in temperature and prolonged heat-treatment time, the sample's crystallinity gradually increases, mirroring the same trend observed in Vickers hardness. It is noteworthy that within the heat-treatment time range of 0–2 h at 800°C, the hardness exhibits minimal variations due to the absence of a significant crystallization [43]. As the temperature and the duration of the thermal treatment increase, the crystallinity tends to rise, contributing positively to the material's hardness. However, if the crystallinity surpasses an optimal threshold, it can introduce structural defects or undesirable crystal arrangements that may compromise the hardness of the sample. This delicate balance highlights the importance of optimizing heat-treatment conditions to achieve the desired crystalline structure and mechanical properties in the G–C [44, 45].

Non-isothermal crystallization kinetics

The conversion (α) in the context of crystallization kinetics refers to the fraction of the material that has undergone a phase transformation from an amorphous to a crystalline state. This transformation is often associated with exothermic peaks observed in the DSC data shown in Fig. 1, acquired at various heating rates ($\beta = 5$, 10, 15, 20, 25, 30, 35, and 40 °C/min). The extent of conversion is a crucial parameter in understanding the kinetics of the crystallization process, and it is calculated using the following equation:

$$\alpha = \frac{\int_{To}^{T}\left(\frac{dHc}{dT}\right)dT}{\int_{To}^{Tf}\left(\frac{dHc}{dt}\right)dT} = \frac{So}{Sf} \tag{9}$$

where *S0* and *Sf* representing the area of DSC heating scans from *To* to *T* and from *To* to *Tf*. The relationship between crystallization time (t) and temperature (T) in the case of non-isothermal crystallization is often expressed using the following equation:

$$t = \frac{|T - T0|}{\beta} \tag{10}$$

where *T0* represents the initial temperature at the commencement of crystallization ($t = 0$), T denotes the temperature at crystallization time t, and β corresponds to the heating rate. Model-free isoconversional methods are commonly employed in the study of thermally activated reactions, particularly in the field of kinetics. These methods aim to determine the *Ea* of a reaction without relying on specific mechanistic details. The two main categories of model-free isoconversional methods are differential and integral methods [46, 47]. Equation (11) describes the crystallization response in all types of non-isothermal kinetics investigations.

Table 3 Effect of heat-treatment time and temperature on c *CrI* and (*d*, *Hv*, *E* and *Y*) of the G-C

Samples	*CrI (%)*	*d (μm)*	*Hv (GPa)*	*E (GPa)*	*Y (GPa)*
800 °C-0 h	0	15.41	0.419 ± 0.01	61.985 ± 1	0.252 ± 0.005
800 °C-1 h	0	14.47	0.425 ± 0.02	70. 3 ± 1	0.286 ± 0.005
800 °C-2 h	48 ± 1	14.25	0.463 ± 0.02	72.484 ± 2	0.295 ± 0.006
800 °C-4 h	56 ± 2	13.93	0.536 ± 0.02	75.856 ± 1	0.308 ± 0.005
800 °C-8 h	67 ± 3	13.35	0.716 ± 0.03	82.59 ± 3	0.336 ± 0.006
800 °C-16 h	86 ± 3	12.71	0.846 ± 0.03	91.117 ± 3	0.371 ± 0.007

$$\frac{d\alpha}{dt} = k(T)f(\alpha) \tag{11}$$

where, $k(T)$ represents the rate constant, $f(\alpha)$ corresponds to the reaction model, and α denotes the conversion rate.

The relationship between temperature, time and conversion rate α is depicted for each heating rate (Fig. 4). It is evident that all samples exhibit a sigmoidal trend in conversion, demonstrating a similar pattern.

Where the rate constant $k(T)$ is governed by the Arrhenius Eq. (12). [48]

$$k(T) = Aexp\left[\frac{-E_a}{RT}\right] \tag{12}$$

where E_a represents the activation energy in (KJ/mol), R is the universal gas constant (8.314 J·mol^{-1}·K^{-1}), T is the absolute temperature in (K), and A is the pre-exponential factor in min^{-1}. The choice of a constant heating rate is common in (DSC) experiments to study kinetic processes; the constant β is defined with:

$$\beta = \frac{dT}{dt} \tag{13}$$

By integrating both the values of $k(T)$ and β into Eq. (1), we can express the modified form of Eq. (14).

$$\frac{d\alpha}{dT} = \left(\frac{A}{\beta}\right)exp\left[\frac{-E_a}{RT}\right]f(\alpha) \tag{14}$$

In order to gain a deeper comprehension of the crystallization kinetics, the crystallization rate expression presented in Eq. (14) signifies the analytical methods utilized to estimate the activation energy Ea through the DSC data [49]. Typically, two main approaches are employed: the model-free and the model-fitting approaches. The latter approach is commonly as it allows for the direct identification of kinetic triplets. Nevertheless, a limitation exists in its incapacity to precisely predict a singular reaction model [50]. On the other hand, isoconversional methods utilize a model independent of varying β but at a constant degree of (α), enabling the prediction of Ea. Model-free methods such as FWO and KAS are examples of isoconversional techniques.

FWO method

The FWO method's strength lies in its ability to assess activation energy at different conversion levels, providing valuable insights into the temperature dependence of reaction rates. The linear segments on the isoconversional plots enable a straightforward determination of activation energy under varying β [51, 52], enhancing the understanding of reaction kinetics, as outlined below:

$$\ln(\beta) = ln\left[A\frac{F_\alpha}{(\frac{d_\alpha}{dt})}\right] - \left[\frac{E_a}{RT}\right] \tag{15}$$

Moreover, by employing Flynn's corrected Doyle's linear approximation [53], the expression for the equation as follows:

$$\ln(\beta) = \left[\ln(\frac{AE}{g(\alpha)R}) - 5.331\right] - \frac{1.052E_a}{RT} \tag{16}$$

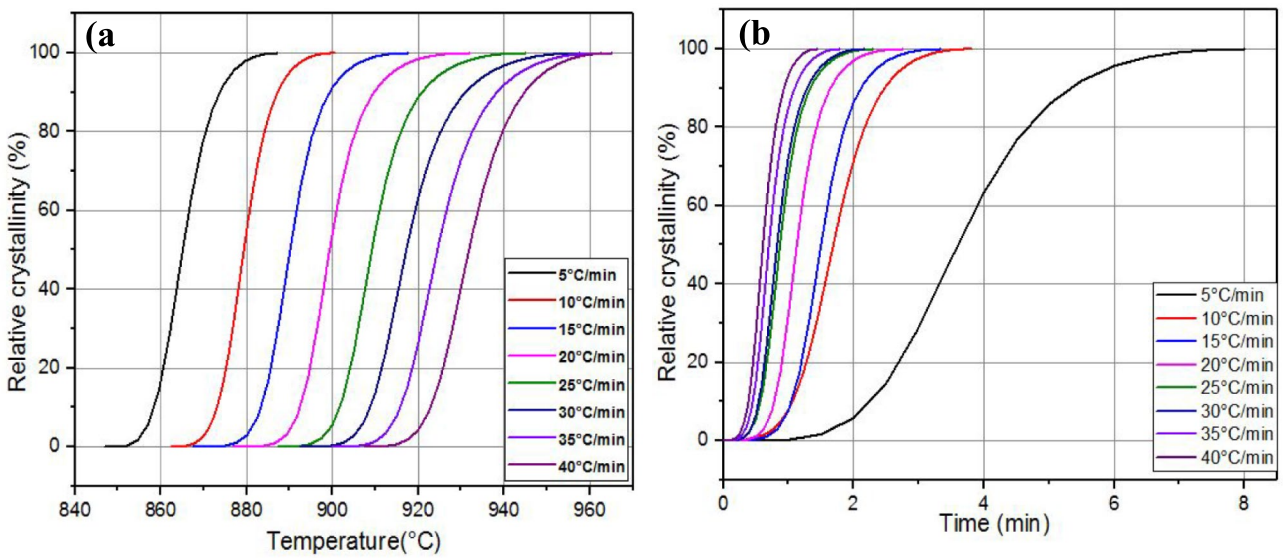

Fig. 4 Relative crystallinity for different heating rates: **a**: A function of temperature (**b**): A function of time

where, *Ea* represents the activation energy, *g(α)* denotes the integral kinetic function, A stands for the pre-exponential factor, and R represents the universal gas constant. Consequently, when *ln (β)* is plotted against *(1/T)*, it should yield linear relationships, allowing us to determine the activation energy through the slope (*-1.052Ea / R*).

KAS method

The KAS method, known for its excellence in integral isoconversional analysis, stands out among the top methods available. This method relies on the numerical approximation of the Arrhenius integral [54]. Like differential methods, the KAS method is a model-free approach, eliminating the need for the explicit identification of the reaction model. Equation (17) represents the final expression of this equation.

$$\ln\left(\frac{\beta}{T^2}\right) = ln\left(\frac{AR}{E_a g(\alpha)}\right) - \frac{E_a}{RT} \tag{17}$$

where, E_a the activation energy, *g(α)* represents the integral conversion function, *A* stands for the pre-exponential factor, and *R* corresponds to the universal gas constant.

Plotting $\ln(\beta/T^2)$ against 1/T at constant conversion (α) using Eq. (17) gives the apparent activation energy from the slope. The FWO and KAS methods were employed to analyze all experimental curves depicted in Figs. 5 and 6 concurrently, the results are listed in Table 4. In both cases (FWO and KAS), the parallel relationship observed in the straight lines contributes valuable insights into the non-isothermal crystallization of G-C, suggesting a uniform and potentially simple reaction mechanism [54–56].

It is evident that the E_a values derived from both approaches (FWO and KAS) are highly similar (296.7 and 294.7 kJ/mol, respectively). This close alignment suggests

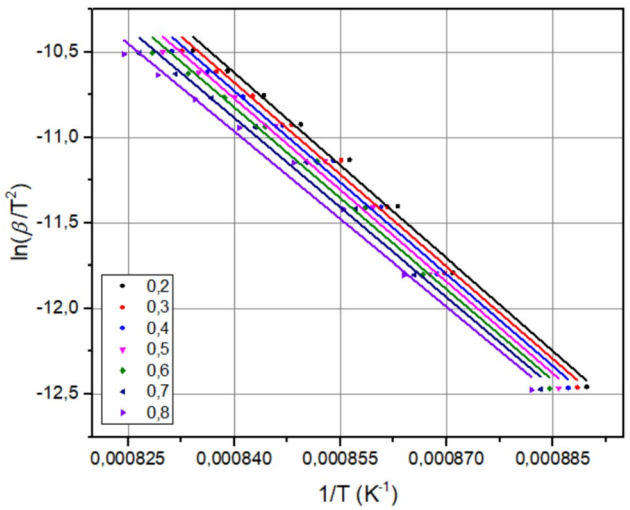

Fig. 5 FOW plots at different *X(T)*

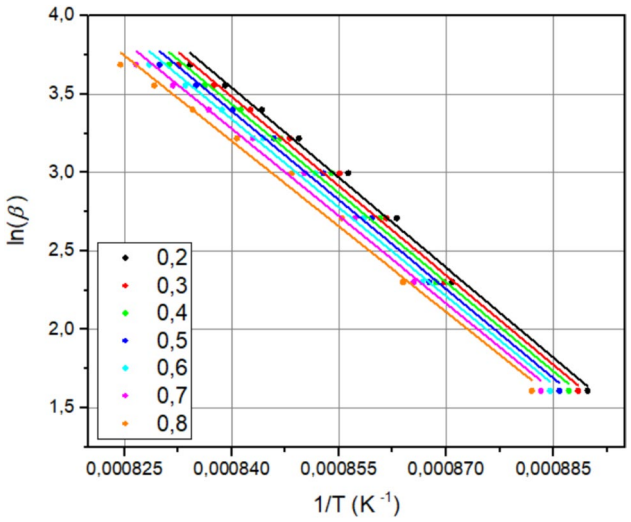

Fig. 6 KAS plots at different *X(T)*

that the E_a for crystallization can be reliably determined using either of these methods. As illustrated in Fig. 7, the outcomes indicate a consistently stable E_α for both methods throughout the entire process, implying that the crystallization of G-C follows a singular step [46]. The R^2 values obtained from both methods, affirm the suitability of both methods for investigating the crystallization kinetics of G–C.

Reaction order and mechanism

The kinetic study involves a comprehensive examination of the rate at which a chemical reaction proceeds over time. This investigation encompasses the determination of reaction order, which quantifies the dependence of the reaction rate on reactant concentrations, as well as the exploration of the reaction mechanism, providing insights into the step-by-step molecular events underlying the reaction. Through experimental measurements and mathematical analyses, the kinetic study aims to elucidate the factors influencing reaction rates and unveil the intricate details of the reaction

Table 4 Variation of *Ea* and average *Ea*, of G-C at different (*α*)

α	FOW method		KAS method	
	Ea (KJ / mol)	R^2	*Ea* (KJ / mol)	R^2
0,2	302.1 ± 2.6	0,99,306	300.6 ± 2.8	0,99,173
0,3	300.1 ± 1.7	0,99,262	298.4 ± 4	0,99,113
0,4	298.9 ± 3.3	0,99,187	297.1 ± 4.9	0,99,019
0,5	298.9 ± 2.9	0,99,125	297.0 ± 3.7	0,98,941
0,6	296.9 ± 3.9	0,99,070	294.7 ± 4.7	0,98,869
0,7	293.2 ± 3.7	0,99,004	290.8 ± 5.3	0,98,786
0,8	286.9 ± 4.2	0,99,011	284.2 ± 4.7	0,98,779
Average	296.7 (± 4.7)		294.7 (± 5.1)	

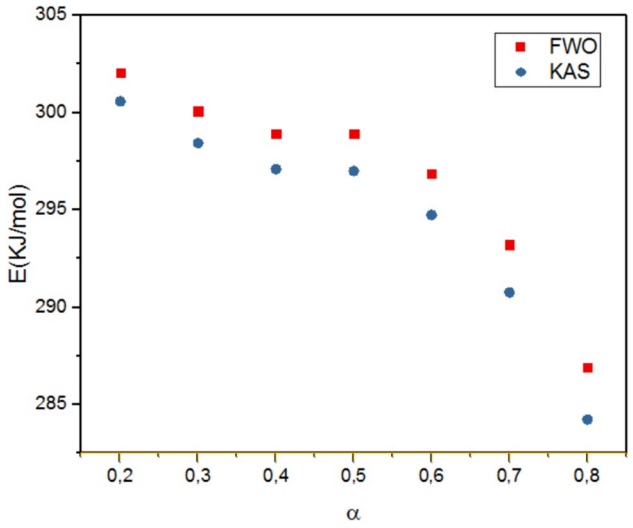

Fig. 7 Variations of *Ea* values as function of (α) of G-C obtained from the FWO and KAS methods

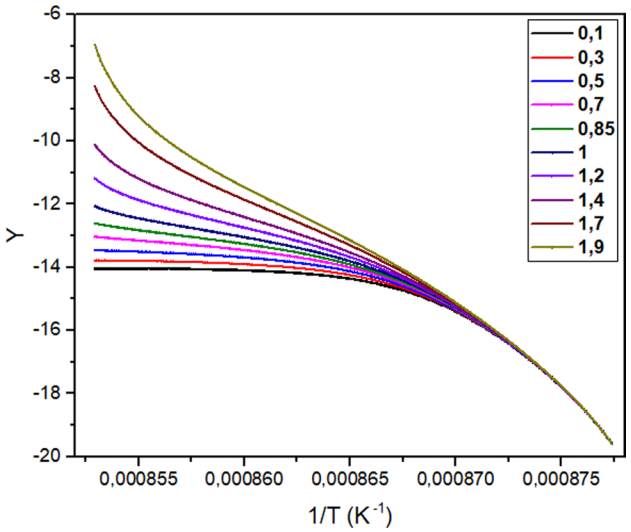

Fig. 8 Determination of *Ea* and reaction rate using C-R method at $\beta = 10$°C/min

pathway, contributing to a deeper understanding of chemical processes [57–59]. The C–R and Criado methods are chosen to determine the kinetic model for the thermal crystallization of G-C because they encompass the crystallization mechanism.

C–R method

The Coats-Redfern (C-R) method is a mathematical approach used to analyze kinetic data and determine the mechanism of a reaction, especially in thermal processes like thermal crystallization of materials [51]. The C-R equations exhibit the following form: [57]

$$Y = ln\left[\frac{1-(1-\alpha)^{1-n}}{(1-n)T^2}\right] = ln\left[\frac{AR}{\beta E_a}\left(1-\frac{2RT}{E_a}\right)\right] - \frac{E_a}{RT} \text{ For n} \neq 1 \quad (18)$$

$$Y = ln\left[\frac{-\ln(1-\alpha)}{T^2}\right] = ln\left[\frac{AR}{\beta E_a}\left(1-\frac{2RT}{E_a}\right)\right] - \frac{E_a}{RT} \text{ For n} = 1 \quad (19)$$

n and β represent the reaction order and heating rate, respectively.

The application of this technique enables the computation of (E_a, pre-exponential factor A, and reaction order (n)) [57]. The *Ea* and *A* factor can be measured by plotting $ln\left[\frac{1-(1-\alpha)^{1-n}}{(1-n)T^2}\right]$ against *1/T*. Equations (18) and (19) demonstrate that $2RT/Ea < 1$. As a result, the entire term can be treated as a constant. [51] The values of *E/R* and *Ln (AR/βE$_a$)* are obtained from the slope and intercept, respectively. The C-R method provides a constant activation energy for a presumed single-step reaction, while the FWO and KAS methods offer activation energy values that vary with conversion, offering a more detailed understanding of the kinetics, especially for reactions with complex mechanisms or multiple steps. Notably, The FWO and KAS methods are robust tools for assessing E_a in a model-free manner, making them suitable for a variety of reactions. However, when it comes to determining reaction order (n), additional considerations and techniques may be necessary, as these methods may not directly provide information about the specific order of the reaction.

The C–R method confirms the selection of the value of (n) when the regression coefficient (R^2) of Eqs. (18) and (19) approaches 1. For this research, diverse reaction orders ranging from $n = 0.1$ to 2.0 are assumed in Eqs. (18) and (19). Figure 8 illustrates the plots with different (n) values, obtained at 10 °C/min. A consistent trend is observed across all curves and heating rates. Table 5 presents the E_a values at various β.

The comparison between E_a values obtained through the C–R method and those from the FWO and KAS methods reveals that the C–R method consistently yields higher values. Nonetheless, it is important to note that despite the disparity, the C-R method shows a similar trend as the FWO and KAS methods. The explanation behind such contrast is that in model fitting approach, different models are fitted to conversion versus temperature curve, and then activation energy and pre-exponential factor are calculated. The disadvantage of this method is that it provides extreme differences in parameters of Arrhenius if a system follows a complex crystallization mechanism [60].

Crystallization mechanism by C–R method

The iso-conversional methods (FWO and KAS) allow for the determination of activation energy at specific values

Table 5 *Ea*, average *Ea*, of G–C determined by C–R method at various β

Coats Redfern method									
b °C/min	5	10	15	20	25	30	35	40	*Ea* average
Ea KJ/mol	399.7±7	387.7±4	371.7±6	359.7±8	343.8±12	327.8±10	311.8±9	295.8±11	349.7 (±34)

of α, whereas the fitting method is advantageous due to its minimal data requirements and the assignment of a single activation energy to an average advancement degree. This method is particularly suited for simple mechanisms. Additionally, the C-R method specified in Eq. (20), finds broad application in ascertaining the most probable crystallization mechanism [57], as stated below.

$$\ln\left(\frac{g(\alpha)}{T^2}\right) = -\frac{Ea}{R}.\frac{1}{T} + ln\frac{AR.\left(1-\frac{2RT}{Ea}\right)}{\beta.Ea} \tag{20}$$

According to the C–R equation, the straight lines should be obtained by fitting the logarithmic term of $g(\alpha)$ over $1/T$ [61]. The most probable function can be identified based on the best value of R^2. Figure 9 exhibits the

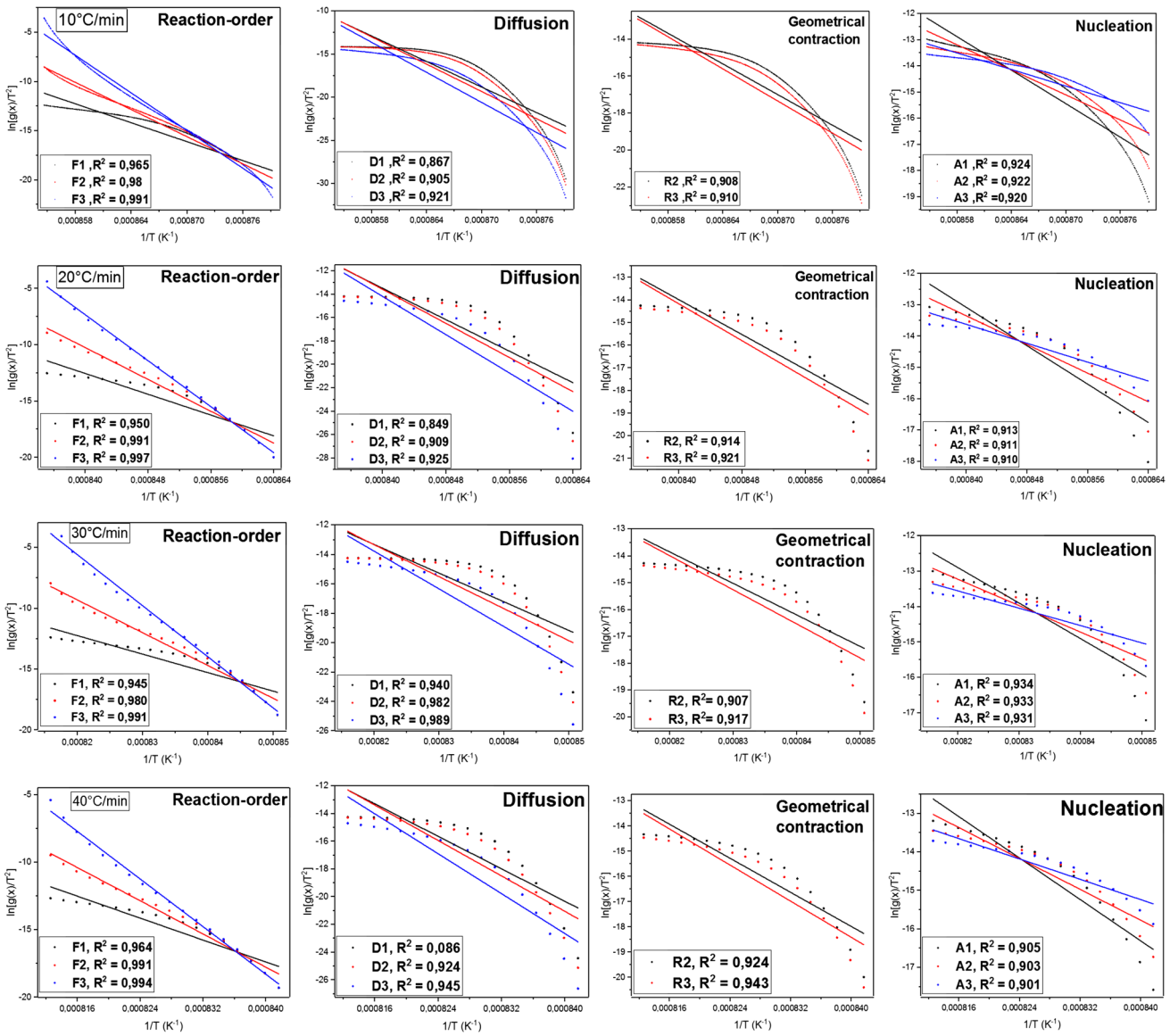

Fig. 9 Fitted results by C–R method at various β

Table 6 *g(a)* and *f(a)* for the prevalent reaction mechanisms in solid-state processes

Mechanism	Solid state process	$f(\alpha)$	$g(\alpha)$
Diffusion D_n	One-dimensional diffusion D1	$\frac{1}{2\alpha}$	α^2
	Two-dimensional diffusion (Valensi model) D2	$[-\ln(1-\alpha)]^{-1}$	$(1-\alpha)\ln(1-\alpha)+\alpha$
	Three dimensioal diffusion (Jander model) D3	$\frac{3}{2}(1-\alpha)^{2/3}\left[1-(1-\alpha)^{1/3}\right]^{-1}$	$\left[1-(1-\alpha)^{1/3}\right]^2$
Reaction order F_n	First order F1	$(1-\alpha)$	$-\ln(1-\alpha)$
	Second order F2	$(1-\alpha)^2$	$\left[(1-\alpha)^{-1}-1\right]$
	Third order F3	$(1-\alpha)^2$	$\left[(1-\alpha)^{-2}-1\right]/2$
Avrami-Erofe've A_n	Avrami- Erofe've A1	$\frac{1}{2}(1-\alpha)[-\ln(1-\alpha)]^{1/3}$	$[-\ln(1-\alpha)]^{2/3}$
	Avrami- Erofe've A2	$2(1-\alpha)[-\ln(1-\alpha)]^{1/2}$	$[-\ln(1-\alpha)]^{1/2}$
	Avrami- Erofe've A3	$3(1-\alpha)[-\ln(1-\alpha)]^{2/3}$	$[-\ln(1-\alpha)]^{1/3}$
Contraction Reaction R_n	Contraction sphere R2	$2(1-\alpha)^{1/2}$	$1-(1-\alpha)^{1/2}$
	Contraction cylinder R3	$3(1-\alpha)^{2/3}$	$1-(1-\alpha)^{1/3}$

fitted plots, which encompass different theoretical functions as per the C–R method. Among them, only the F3 kinetic model demonstrates an excellent linear fit with a high R^2 value (0.999). This suggests that, in the experimental context, the F3 model provides a particularly accurate representation of the observed data when fitting the C-R equation.

The F3 model proposes that within the solid-state reaction, the nucleation process involves the simultaneous formation of three nuclei. This simultaneous initiation sets it apart from other kinetic models that may involve different nucleation patterns [62].

Confirmation of crystallization mechanism

In this investigation, the Criado method was employed to validate the accuracy of the kinetic model and ascertain the corresponding kinetic parameters [63]. Equation (21) can be utilized to calculate the experimental values in the following manner:21 where, *p(x)* can be obtained from Eq. (22), considering a minimal error level $10^{-5}\%$ for $x > 20$ [64]:

$$p(x) = \frac{e^{-x}}{x}\frac{x^3 + 18x^2 + 86x + 96}{x^4 + 20x^3 + 120x^2 + 240x + 120} \tag{22}$$

where, x is E_a/RT.

By applying Eq.23 and the corresponding $g(\alpha)$ and $f(\alpha)$ values obtained from Table 6, theoretical master plots were constructed. These plots illustrate $Z(\alpha)$ against (α) for various reaction mechanisms, including reaction order, diffusion, geometric contraction, and nucleation, as categorized [62]:

$$Z(\alpha)_{theortical} = g(\alpha)f(\alpha) \tag{23}$$

After obtaining the experimental curves, they are compared with various theoretical master plots to determine the appropriate thermal crystallization mechanism. The activation energy (E_a) and pre-exponential factor (A), determined using the Coats-Redfern (C-R) method, are used to plot master curves for glass ceramics, which illustrate the thermal crystallization mechanism. Figure 10 illustrates the calculated $Z(\alpha)_{exp}$ plots, which serve as a straightforward and precise means of identifying the crystallization mechanism by matching them with the master plots.

The matching point is evidently *F3*, for advanced conversion rates. This shift occurs at an approximate temperature of 800 °C, where the higher temperature can accelerate the crystallization process in glass ceramics. When glass is heated a 800 °C, it undergoes controlled nucleation and growth of crystals, converting it into a glass ceramic material. The increased temperature provides more thermal energy to the atoms and molecules within the glass, facilitating their rearrangement and formation of crystal nuclei. As the temperature continues to rise, the crystal growth becomes more pronounced, resulting in a well-defined crystalline structure. This controlled crystallization imparts specific properties and advantages to glass ceramics, such as increased strength and improved thermal stability [65, 66].

Conclusion

In this comprehensive experimental study has provided valuable insights into the nucleation and growth processes of crystalline phases within a lithium aluminosilicate glass containing 2.5 wt% TiO_2 and 2.5 wt%

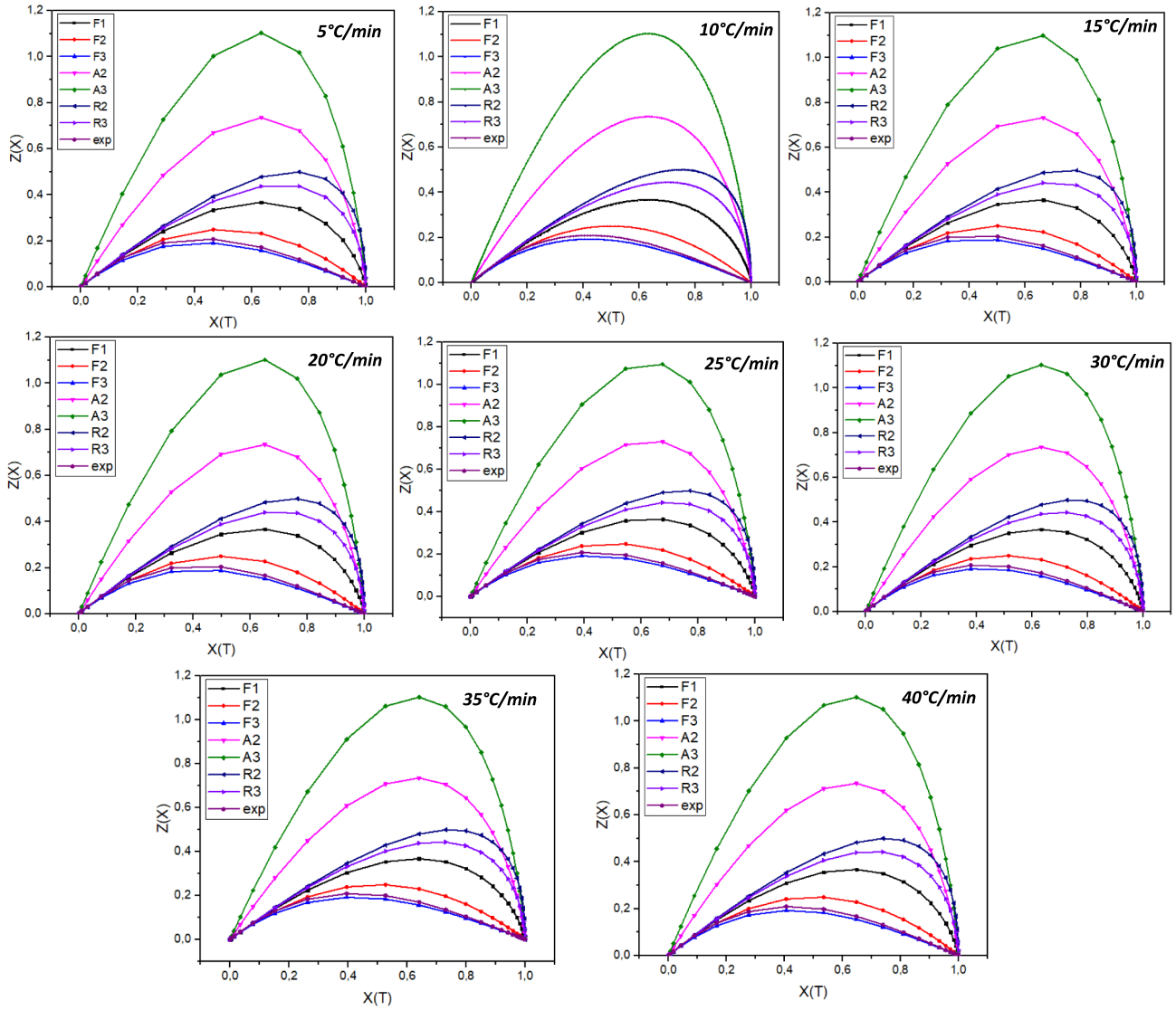

Fig. 10 Reaction mechanism plots at different β by Criado method

ZrO_2 as a nucleating agent. The successful fabrication of a fully dense glass–ceramic with a virgilite crystalline phase ($Li_x\ Al_x\ Si_{3-x}\ O_6$) was achieved at an approximate temperature of 800 °C. Subsequent heat treatment resulted in a substantial enhancement of microhardness and crystallinity index, while the elastic modulus and yield strength parameter exhibited an increase proportionate to the observed hardness rise.

The application of DSC under non-isothermal conditions proved effective in investigating the Crystallization Kinetics of the glass–ceramic. This approach enabled the determination of crucial kinetic parameters, including the E_α and kinetic model ($f\alpha$). Remarkably similar average Ea values were obtained using the FWO and KAS methods, measuring at 296,7 and 294,7 kJ/mol, respectively. This consistency suggests the reliability of calculating the activation energy of crystallization using either of these two methods. The findings contribute to a deeper understanding of the thermal and mechanical properties of the fabricated glass–ceramic, providing valuable information for future applications and advancements in materials science.

In this study, the crystallization mechanism was confirmed by C–R and Criod methods. The non-isothermal crystallization kinetics adhere to a Third Order Reaction ($F3$) characterized by both integral ($g(a) = (1-\alpha)^2$) and differential ($f(a) = \frac{[(1-\alpha)^{-2}-1]}{2}$) forms. The $F3$ reaction model implies a random nucleation process where three nuclei concurrently form within each individual particle. This mechanism entails the simultaneous formation of three nuclei, introducing potential implications for the overall reaction kinetics and mechanism.

Acknowledgements The authors extend our sincere gratitude to Dr. C. MAÏ from MATEIS-l'INSA Lyon and G. ANDRIEU from the "Centre de Recherche Corning Europe" for their invaluable contribution in providing the initial glass used in our research.

Author contributions A. Layachi, S. Satha and H. Satha: Methodology, A. Layachi, H. Satha and M.F. Gonon: investigation, A. Layachi and H. Satha: writing—original draft preparation, A. Layachi, H. Satha: writing—review and editing, A. Layachi, S. Satha H. Satha, and M.F. Gonon: supervision. All authors have read and agreed to the published version of the manuscript.

Funding This research received no external funding.

Data availability All data generated or analyzed during this study are included in this published article.

Declarations

Competing interests The authors declare that they have no known competing financial interests or personal relationships that could have appeared to influence the work reported in this paper.

References

1. Orlova, L.A., Chainikova, A.S., Alekseeva, L.A., Voropaeva, M.V.: Voropaeva, Recent advances in radio transparent glass-ceramic materials based on high-temperature aluminosilicate systems. Russ. J. Inorg. Chem. **60**(13), 1692–1707 (2015). https://doi.org/10.1134/S0036023615130045
2. Han, L., Song, J., Zhang, Q., Luo, Z., Lu, A.: Crystallization, structure and characterization of MgO-Al2O3-SiO2-P2O5 transparent glass-ceramics with high crystallinity. J. Non-Cryst. Solids **481**, 123–131 (2018). https://doi.org/10.1016/j.jnoncrysol.2017.10.028
3. Ohsato, H., Kim, J.S., Cheon, C.I., Kagomiya, I.: Crystallization of indialite/cordierite glass-ceramics for millimeter-wave dielectrics. Ceram. Int. **41**, S588–S593 (2015). https://doi.org/10.1016/j.ceramint.2015.03.140
4. Marghussian, V.K., Balazadegan, O.U., Eftekhari-Yekta, B.: Crystallization behavior, microstructure and mechanical properties of cordierite–mullite glass-ceramics. J. Alloys Compd. **484**(1–2), 902–906 (2009). https://doi.org/10.1016/j.jallcom.2009.05.080
5. Sohn, S.B., Choi, S.Y., Lee, Y.K.: Controlled crystallization and characterization of cordierite glass-ceramics for magnetic memory disk substrate. J. Mater. Sci. **35**, 4815–4821 (2000). https://doi.org/10.1023/A:1004876829705
6. Hao, X., Hu, X., Luo, Z., Liu, T., Li, Z., Wu, T., Tang, Y.: Preparation and properties of transparent cordierite-based glass-ceramics with high crystallinity. Ceram. Int. **41**(10), 14130–14136 (2015). https://doi.org/10.1016/j.ceramint.2015.07.034
7. Pannhorst, W.: Glass ceramics: state-of-the-art. J. Non-Cryst. Solids **219**, 198–204 (1997). https://doi.org/10.1016/S0022-3093(97)00270-6
8. Gonon, M., Satha, S., Zanin, T., Satha, H., Abdelouhab, S.: Sr2TiSi2O8 (STS) Polar Glass-Ceramics: Effect of Na2O and CaO Additions in the Parent Glass on the Crystallization Mechanism and on the Piezoelectric Properties. Ceramics **6**(1), 1–15 (2023). https://doi.org/10.3390/ceramics6010001
9. Zanotto, E.D.: A bright future for glass-ceramics. Am. Ceram. Soc. Bull. **89**(8), 19–27 (2010)
10. Holand, W., Beall G.H.: Glass-Ceramic Technology, 2nd ed., John Wiley & Sons Inc Hoboken NJ (2019)
11. Henderson, D.: Experimental analysis of non-isothermal transformations involving nucleation and growth. J. Therm. Anal. **15**, 325–331 (1979). https://doi.org/10.1007/BF01903656
12. Al-Harbi, O.A.: Effect of different nucleation catalysts on the crystallization of Li2O–ZnO–MgO–Al2O3–SiO2 glasses. Ceram. Int. **35**(3), 1121–1128 (2009). https://doi.org/10.1016/j.ceramint.2008.05.008
13. Alekseeva, I., Dymshits, O., Tsenter, M., Zhilin, A.: Influence of various alkali and divalent metal oxides on phase transformations in NiO-doped glasses of the Li2O–Al2O3–SiO2–TiO2 system. J. Non-Cryst. Solids **357**(11–13), 2209–2214 (2011). https://doi.org/10.1016/j.jnoncrysol.2010.12.065
14. Hunger, A., Carl, G., Rüssel, C.: Formation of nano-crystalline quartz crystals from ZnO/MgO/Al2O3/TiO2/ZrO2/SiO2 glasses. Solid State Sci. **12**(9), 1570–1574 (2010). https://doi.org/10.1016/j.solidstatesciences.2010.06.025
15. Pinckney, L.R., Beall, G.H.: Microstructural evolution in some silicate glass-ceramics: a review. J. Am. Ceram. Soc. **91**(3), 773–779 (2008). https://doi.org/10.1111/j.1551-2916.2007.02129.x
16. Shearer, A., Montazerian, M., Deng, B., Sly, J.J., Mauro, J.C.: Zirconia-containing glass-ceramics: From nucleating agent to primary crystalline phase. Int. J. Ceram. Eng. Sci. **6**(2), e10200 (2024). https://doi.org/10.1002/ces2.10200
17. Guo, X., Yang, H., Cao, M.: Nucleation and crystallization behavior of Li2O–Al2O3–SiO2 system glass–ceramic containing little fluorine and no-fluorine. J. Non-Cryst. Solids **351**(24–26), 2133–2137 (2005). https://doi.org/10.1016/j.jnoncrysol.2005.04.071
18. Höche, T., Mäder, M., Bhattacharyya, S., Henderson, G.S., Gemming, T., Wurth, R., Avramov, I.: ZrTiO 4 crystallisation in nanosized liquid–liquid phase-separation droplets in glass—a quantitative XANES study. Cryst. Eng. Comm **13**(7), 2550–2556 (2011). https://doi.org/10.1039/C0CE00716A
19. Höche, T., Patzig, C., Gemming, T., Wurth, R., Rüssel, C., Avramov, I.: Temporal evolution of diffusion barriers surrounding ZrTiO4 nuclei in lithia aluminosilicate glass-ceramics. Cryst. Growth Des. **12**(3), 1556–1563 (2012). https://doi.org/10.1021/cg2016148
20. de Pablos-Martín, A., Hémono, N., Mather, G.C., Bhattacharyya, S., Höche, T., Bornhöft, H., Pascual, M.J.: Crystallization kinetics of LaF3 nanocrystals in an oxyfluoride glass. J. Am. Ceram. Soc. **94**(8), 2420–2428 (2011). https://doi.org/10.1111/j.1551-2916.2011.04547.x
21. Guo, X., Yang, H., Han, C., Song, F.: Crystallization and microstructure of Li2O–Al2O3–SiO2 glass containing complex nucleating agent. Thermochim. Acta **444**(2), 201–205 (2006). https://doi.org/10.1016/j.tca.2006.02.016
22. Li, Y., Xu, B., Cao, J., Liang, L., Liang, K.: Effect of MgO addition on crystallization and microstructure of Li2O–Al2O3–SiO2 Ta2O5 glassceramics. Phys. Chem. Glasses: Eur. J. Glass. Sci. Technol. Part B. **51**(3), 173–178 (2010)
23. Matusita, K., Sakka, S.: Kinetic study on crystallization of glass by differential thermal analysis-criterion on application of kissinger plot. J. Non-Cryst. Solids **38**, 741–746 (1980). https://doi.org/10.1016/0022-3093(80)90525-6
24. Wang, M.C., Li, W.L., Cheng, C.W., Chang, K.M., Chen, Y.F., Hsi, C.: S, The phase transformation and crystallization kinetics of (1x) Li2O–xNa2O–Al2O3–4SiO2 glasses. Mater. Chem. Phys. **123**(1), 203–209 (2010). https://doi.org/10.1016/j.matchemphys.2010.03.083
25. Fernandes, H.R., Tulyaganov, D.U., Goel, I.K., Ferreira, J.M.: Crystallization process and some properties of Li2O–SiO2 glass ceramics doped with Al2O3 and K2O. J. Am. Ceram. Soc. **91**, 3698–3703 (2008). https://doi.org/10.1111/j.1551-2916.2008.02724.x

26. Barbieri, L., Leonelli, C., Manfredini, T., Siligardi, C., Corradi, A.B., Mustarelli, P., Tomasi, C.: Nucleation and crystallization of a lithium aluminosilicate glass. J. Am. Ceram. Soc. **91**(11), 3698–3703 (2008). https://doi.org/10.1111/j.1151-2916.1997.tb03235.x
27. Ray, C.S., Day, D.E.: Determining the nucleation rate curve for lithium disilicate glass by differential thermal-analysis. J. Am. Ceram. Soc. **73**, 439–442 (1990). https://doi.org/10.1111/j.1151-2916.1990.tb06532.x
28. Kim, K.D., Lee, S.H., Ahn, H.K.: Observation of nucleation effect on crystallization in lithium aluminosilicate glass by viscosity measurement. J. Non-Cryst. Solids **73**(2), 439–442 (1990). https://doi.org/10.1016/j.jnoncrysol.2004.01.001
29. Chen, M., He, F., Shi, J., Xie, J., Yang, H., Wan, P.: Low Li2O content study in Li2O-Al2O3-SiO2 glass-ceramics. J. Eur. Ceram. Soc. **39**(15), 4988–4995 (2019). https://doi.org/10.1016/j.jeurceramsoc.2019.07.032
30. Venkateswaran, C., Sreemoolanadhan, H., Pant, B., Sharma, S. C., Chauhan, V. S., Vaish, R., Vaish, R.: Processing Li2O-Al2O3-SiO2 (LAS) glass-ceramic with and without P2O5 through bulk and sintering route, J. Non-Cryst. Solids. **550**, 120289 (2020). https://doi.org/10.1016/j.jnoncrysol.2020.120289
31. Mai, C., Satha, H., Thollet, G., Vigier, G., Andrieu, G.: Saxs, waxd and tem of the early stages of crystallization in TiO2-ZrO2-MgO-Li2O-Al2O3-SiO2 glass. J. Non-Cryst. Solids **108**(2), 201–206 (1989). https://doi.org/10.1016/0022-3093(89)90584-X
32. Krimm, S., Tobolsky, A. V.: Quantitative X-ray studies of order in amorphous and crystalline polymers. Quantitative X-ray determination of crystallinity in polyethylene. J. Polym. Sci. **7**(1), 57–76 (1951). https://doi.org/10.1002/pol.1951.120070105
33. Ozturk, O., Asikuzun, E., Kaya, S., Yildirim, G., Turkoz, M.B., Kilic, A.: Improvement of the nature of indentation size effect of Bi-2212 superconducting matrix by doped Nd inclusion and theoretical modeling of new matrix. J. Supercond. Novel Magn. **27**, 1403–1412 (2014). https://doi.org/10.1007/s10948-014-2477-4
34. Asikuzun, E., Ozturk, O., Cetinkara, H.A., Yildirim, G., Varilci, A., Yılmazlar, M., Terzioglu, C.: Vickers hardness measurements and some physical properties of Pr2O3 doped Bi-2212 superconductors. J. Mater. Sci. Mater. Electron. **23**, 1001–1010 (2012). https://doi.org/10.1007/s10854-011-0537-0
35. Oliver, W.C., Pharr, G.M.: An improved technique for determining hardness and elastic modulus using load and displacement sensing indentation experiments. J. Mater. Res. **7**(6), 1564–1583 (1992). https://doi.org/10.1557/JMR.1992.1564
36. Tabor, D.: The hardness and strength of metals. J. Inst. Met. **79**, 1 (1951)
37. Muiva, C.M., Sathiaraj, S.T., Mwabora, J.M.: Crystallisation kinetics, glass forming ability and thermal stability in glassy Se100 – x Inx chalcogenide alloys. J. Non-Cryst. Solids **357**(22–23), 3726–3733 (2011). https://doi.org/10.1016/j.jnoncrysol.2011.07.033
38. Banijamali, S.: Ebadzadeh, Glass-forming ability, sinter-crystallization behavior and microwave dielectric properties of MgO-B2O3-(Al2O3)-SiO2 glass-ceramics. J. Non-Cryst. Solids **441**, 34–41 (2016). https://doi.org/10.1016/j.jnoncrysol.2016.03.014
39. Hesse, K.F., Liebau, F.: Crystal chemistry of silica-rich Barium silicates III: refinement of the crystal structures of the layer silicates Ba2(Si4O10) (I), (Sanbornite), and Ba2(Si4O10) (h). Z. Kristallogr. **153**(1–2), 33–41 (1980). https://doi.org/10.1524/zkri.1980.0004
40. Haller, W., Blackburn, D. H., Simmons, J. H.: Miscibility gaps in alkali-silicate binaries—data and thermodynamic interpretation. J. Am. Ceram. Soc. **57**(3), 120–126 (1974). https://doi.org/10.1111/j.1151-2916.1974.tb10832.x
41. Khater, G.A., Idris, M.H.: Role of TiO2 and ZrO2 on crystallizing phases and microstructure in Li. Ba aluminosilicate glass. Ceram. Int. **33**(2), 233–238 (2007). https://doi.org/10.1016/j.ceramint.2005.08.016
42. Fernandes, H.R., Tulyaganov, D.U., Ferreira, J.M.: The role of P_2O_5, TiO_2 and ZrO_2 as nucleating agents on microstructure and crystallization behaviour of lithium disilicate-based glass. J. Mater. Sci. **48**, 765–773 (2013). https://doi.org/10.1007/s10853-012-6793-4
43. Banijamali, S., Yekta, B.E., Rezaie, H.R., Marghussian, V.K.: Marghussian, Marghussian, Crystallization and sintering characteristics of CaO–Al2O3–SiO2 glasses in the presence of TiO2, CaF2 and ZrO2. Thermochim. Acta **488**(1–2), 60–65 (2009). https://doi.org/10.1016/j.tca.2008.12.031
44. Zhang, S., Zhang, Y., Gao, J., Qu, Z., Zhang, Z.: Effects of Cr2O3 and CaF2 on the structure, crystal growth behavior, and properties of augite-based glass ceramics. J. Eur. Ceram. Soc. **39**(14), 4283–4291 (2019). https://doi.org/10.1016/j.jeurceramsoc.2019.05.060
45. Hou, Y., Zhang, G.H., Chou, K.C., Fan, D.: Effects of CaO/SiO2 ratio and heat treatment parameters on the crystallization behavior, microstructure and properties of SiO2-CaO-Al2O3-Na2O glass ceramics. J. Non-Cryst. Solids **538**, 120023 (2020). https://doi.org/10.1016/j.jnoncrysol.2020.120023
46. Rezaei-Shahreza, P., Seifoddini, A., Hasani, S.: Thermal stability and crystallization process in a Fe-based bulk amorphous alloy: the kinetic analysis. J. Non-Cryst. Solids **471**, 286–294 (2017). https://doi.org/10.1016/j.jnoncrysol.2017.05.044
47. Vyazovkin, S., Burnham, A.K., Criado, J.M., Pérez-Maqueda, L.A., Popescu, C., Sbirrazzuoli, N.: ICTAC kinetics Committee recommendations for performing kinetic computations on thermal analysis data. Thermochim. Acta **520**(1–2), 1–19 (2011). https://doi.org/10.1016/j.tca.2011.03.034
48. Kumar, A., Chakrabarti, A., Shekhawat, M.S., Molla, A.R.: Transparent ultra-low expansion lithium aluminosilicate glass-ceramics: Crystallization kinetics, structural and optical properties. Thermochimi. Acta. **676**, 155–163 (2019). https://doi.org/10.1016/j.tca.2019.04.006
49. Ghasemzadeh, M., Nemati, A., Nozad, A., Hamnabard, Z., Baghshahi, S.: Crystallisation kinetics of glass-ceramics by differential thermal analysi. Ceram. Silik. **55**, 188–194 (2011)
50. Khawam, A., Flanagan, D.R.: Complementary use of model-free and modelistic methods in the analysis of solid-state kinetics. J. Phys. Chem. B **55**(2), 188–194 (2011). https://doi.org/10.1021/jp050589u
51. Ozawa, T.: Kinetic analysis of derivative curves in thermal analysis. J. Therm. Anal. **2**, 301–324 (1970). https://doi.org/10.1007/BF01911411
52. Păcurariu, C., Lazău, R., Lazău, I., Ianoş, R., Tiţa, B.: Non-isothermal crystallization kinetics of some basaltic glass-ceramics containing CaF 2 as nucleation agent. J. Therm. Anal. Calorim. **97**(2), 507–513 (2009). https://doi.org/10.1007/s10973-009-0369-9
53. Flynn, J.H.: The isoconversional method for determination of energy of activation at constant heating rates. J. Therm. Anal. **27**, 95–102 (1983). https://doi.org/10.1007/BF01907325
54. Shi, J., He, F., Xie, J., Liu, X., Yang, H.: Yang, Kinetic analysis of crystallization in Li2O-Al2O3-SiO2-B2O3-BaO glass-ceramics. J. Non-Cryst. Solids **491**, 106–113 (2018). https://doi.org/10.1016/j.jnoncrysol.2018.04.004
55. Boucenna, Y., Layachi, A., Cherfia, A., Laoutid, F., Satha, H.: Non-Isothermal Crystallization Kinetics and Activation Energy for Crystal Growth of Polyamide 66/Short Glass Fiber/Carbon Black Composites. Materials **16**(22), 7073 (2023). https://doi.org/10.3390/ma16227073

56. Gharsallah, A., Layachi, A., Louaer, A., Satha, H.: Thermal degradation kinetics of Opuntia Ficus Indica flour and talc-filled poly (lactic acid) hybrid biocomposites by TGA analysis. J. Compos. Mater. **55**(22), 3099–3118 (2021). https://doi.org/10.1177/00219983211008202
57. Coats, A.W., Redfern, J.P.: Kinetic parameters from thermogravimetric data. Nature **201**(4914), 68–69 (1964). https://doi.org/10.1038/201068a0
58. Flynn, J. Wall, L.: A quick, direct method for the determination of activation energy from thermogravimetric data. J. Polym. Sci. B Polym. Lett.**4**, 323–328 (1966).https://doi.org/10.1002/pol.1966.110040504
59. Savabieh, H., Alizadeh, P., Nayebi, B., Clemens, F. J.: Kinetics of crystallization in 13.2 Li2O-67.6 SiO2–14.49 Al2O3–3.3 TiO2–0.4 BaO-0.97 ZnO glass ceramic powder: Part I: A model-free vs. model-fitting approach. Ceram. Int. **45**(7), 8856–8865 (2019). https://doi.org/10.1016/j.ceramint.2019.01.214
60. Aboyade, A.O., Carrier, M., Meyer, E.L., Knoetze, J.H., Görgens, J.F.: Model fitting kinetic analysis and characterisation of the devolatilization of coal blends with corn and sugarcane residues. Thermochim. Acta **530**, 95–106 (2012). https://doi.org/10.1016/j.tca.2011.12.007
61. Criado, J.M., Malek, J., Ortega, A.: Applicability of the master plots in kinetic analysis of non-isothermal data. Thermochim. Acta **147**(2), 377–385 (1989). https://doi.org/10.1016/0040-6031(89)85192-5
62. Bezerra, G.V., Cabral, A.A.: Model-free and model-fitting analysis applied to the non-isothermal crystallization kinetics of a SrO-CaO-B2O3-TiO2-SiO2 glass sealant for SOFCs. J. Non-Cryst. Solids **572**, 121113 (2021). https://doi.org/10.1016/j.jnoncrysol.2021.121113
63. Senum, G.I.: Yang, Rational approximations of the integral of the Arrhenius function. J. Therm. Anal. **11**(3), 445–447 (1977). https://doi.org/10.1007/BF01903696
64. Khawam, A., Flanagan, D.R.: Solid-state kinetic models: basics and mathematical fundamentals. J. Phys. Chem. B **110**(35), 17315–17328 (2006). https://doi.org/10.1021/jp062746a
65. Kothiyal, G.P., Ananthanarayanan, A. Dey, G.K.: Glass and glass-ceramics. Functional Materials Preparation, Processing and Applications, 323–386 (2012)
66. Smiljanić, S.V., Grujić, S.R., Tošić, M.B., Živanović, V.D., Stojanović, J.N., Matijašević, S.D., Nikolić, J.D.: Crystallization and sinterability of glass-ceramics in the system La2O3–SrO–B2O3. Ceram. Int. **40**(1), 297–305 (2014). https://doi.org/10.1016/j.ceramint.2013.06.002